Results in Engineering 27 (2025) 106598

Contents lists available at ScienceDirect

Results in Engineering

journal homepage: www.sciencedirect.com/journal/results-in-engineering

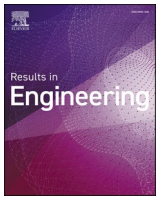

Research paper

Deep learning-based thermal modeling of slipping velocity in oblique magnetohydrodynamic non-Newtonian nanofluid flows

Nek Muhammad Katbar [a,b,*], Hina Zahir [c], Kamel Guedri [d], Basim M. Makhdoum [d], Siti Suzilliana Putri Mohamed Isa [e,f], Syed M. Hussain [g], Abbas Khan [h]

[a] School of Mathematics and Statistics, Central South University, Changsha 410083, China
[b] Department of Mathematics, Mehran UET Shaheed Zulfiqar Ali Bhutto Campus Khairpur, Pakistan
[c] Department of Mathematics, Shaheed Benazir Bhutto Woman University Peshawar, Pakistan
[d] Mechanical Engineering Department, College of Engineering and Architecture, Umm Al-Qura University, P. O. Box 5555, Makkah 21955, Saudi Arabia
[e] Centre for Foundation Studies in Science of Universiti Putra Malaysia, Universiti Putra Malaysia, 43400 UPM Serdang, Selangor, Malaysia
[f] Institute for Mathematical Research, Universiti Putra Malaysia, 43400 UPM Serdang Selangor, Malaysia
[g] Department of Mathematics, Faculty of Science, Islamic University of Madinah, Madinah 42351, Saudi Arabia
[h] Department of Mathematics & Statistics, University of Haripur, Haripur, KP 22620, Pakistan

ARTICLE INFO

Keywords:
Deep learning
Carreau nanofluid
Roseland approximation
Inclined magnetic field
Velocity slip

ABSTRACT

In recent years, artificial neural networks (ANNs) have emerged as reliable and efficient computational tools for solving highly nonlinear and complex mathematical models in fluid dynamics. Motivated by the limitations in existing studies on nanofluid flows under magnetic influence, this work investigates the inclined magnetohydrodynamic (MHD) flow of a Carreau nanofluid incorporating cubic autocatalysis and homogeneous heterogeneous chemical reactions. The physical model considers temperature-dependent thermal conductivity and a magnetized environment to better capture real-world transport phenomena. A system of partial differential equations (PDEs) governing the flow, heat, and mass transfer is formulated and reduced to a set of ordinary differential equations (ODEs) using similarity transformations, with boundary conditions imposed over the interval [0, ∞).

The resulting ODEs are solved using the Artificial Neural Network (ANN) approach, with the MATLAB-based bvp4c solver employed for validation. Statistical comparisons confirm the accuracy of ANN with a mean square error below 10^-5. The results reveal that an increase in the homogeneous reaction parameter enhances nanoparticle dispersion, thereby increasing the nanofluid temperature by approximately 18.6 % for the shear-thinning case and 22.3 % for the shear-thickening case. Moreover, the application of a stronger magnetic field intensifies the Lorentz force, leading to a 27 % reduction in velocity. The findings demonstrate the robust influence of chemical reactions and magnetic forces on heat and mass transport in non-Newtonian nanofluids, offering valuable insights for industrial and biomedical applications.

1. Introduction

Recently, the experimental and theoretical research in non-Newtonian fluids are expanding due to their significant application in the industrial field and engineering. Some of the manufactured non-Newtonian fluid are shampoo, starch, cocoa, toothpaste, jelly, etc. Since the correlation between 2 variables (shear stress and shear rate) in the non-Newtonian is indirectly proportional with each others, then it is appropriate to introduce the rheological properties, which these properties describe the stress and strain rate tensors under the limitations of specific fluid flow. Rheological properties describe the effect of the forces acts on the fluid, and causes the fluid shape to change [1,2]. The Newtonian and non-Newtonian fluid are differentiated regarding the relationship between deformation rate and shear rate: the linear relationship is owned by Newtonian fluid, whereas the nonlinear relation is showed by non-Newtonian fluid. However, the type of fluid which owns the very high and very low shear rates is known as Carreau fluid [3]. The studies regarding Carreau fluid and another fluidic attitude with different facts have been reported [4–6]. Different effected parameters and dissimilarities flow shapes were studied, but the common factor was that the fluid was Carreau-type and multiple numerical methods were

* Corresponding author at: School of Mathematics and Statistics, Central South University, Changsha 410083, China.
E-mail address: nalhbshi@yahoo.com (N.M. Katbar).

https://doi.org/10.1016/j.rineng.2025.106598
Received 22 June 2025; Received in revised form 26 July 2025; Accepted 3 August 2025
Available online 5 August 2025

Nomenclature

γ_0	length of slip
n	Carreau fluid index
B_0	strength of magnetic field
k	thermal conductivity
τ	ratio parameter
C	liquid concentricity
T	liquid temperature
D_B	Brownian diffusion
D_T	thermophoresis coefficient
T_∞	temperature noted at infinity
T_f	Plate temperature
ϑ	angle of projected magnetic field
ρ_f	fluid density
γ	velocity slip parameter
α	thermal diffusivity
c_p	specific heat
M	magnetic variable
Q^*	heat generating/sink variable
Q	heat sink/source parameter
X	reaction rate parameter
E, F	Autocatalysis
G_a, G_b	concentricity of chemical reactions
k_1, k_s	homo/heterogeneous reactions rate
ΔH_h	homogeneous heat reaction
BLMS	Backpropagated Levenberg-Marquard scheme
CFMNM	Carreau fluid Magneto-nanofluidic model
D_A	heterogeneous reaction stoichiometric coefficient
u, v, w	velocity component
x, y, z	space coordinates
σ^*, k^*	Stefan Boltzmann constant
Pr	NotationPrandtl number
Nb	Brownian motion symbol
Nt	thermophoresis parameter
Le	Lewis number
We_1, We_2	local Weissenberg number
Bi	Biot quantity
u_w, v_w	Plate velocity in x- and y- axes
Nr	radiation parameter
υ	kinematic viscosity
c_f	skin-friction coefficient
Nu_x	Nusselt number
Re_x	local Reynold number
σ_1	reaction rate of electricity
λ	velocity ratio parameter
Δ	chemical reaction constant
ε	diffusion coefficient
R_H	homogenous reaction
f, g	dimensionless velocities
K_T	thermal conductivity
NN	Neural Network
MNM	Magneto-nanofluidic model

used in these previous studies [4–6]. Recently, the additional effects of motile gyrotactic micro-organisms [7], stagnation point flow [8,9], thermophoresis and Brownian motion [10], and thermal radionuclides [6] in the Carreau fluid flow have explored by Hosseinzadeh et al. [7], Hayat et al. [8], Waqas et al. [9], by Sultan et al. [10], and Shaw et al. [11].

The concentration of the fluid is determined by the involved mechanisms of that fluid in the environment and industries. In addition, the chemical reaction whether the reaction is homogenous or heterogeneous will affect the fluid flow [12]. Some of the associated chemical processes involves the technologies in the food preparation, glassware or ceramics manufacturing, and polymeric synthesis. Many studies have recently

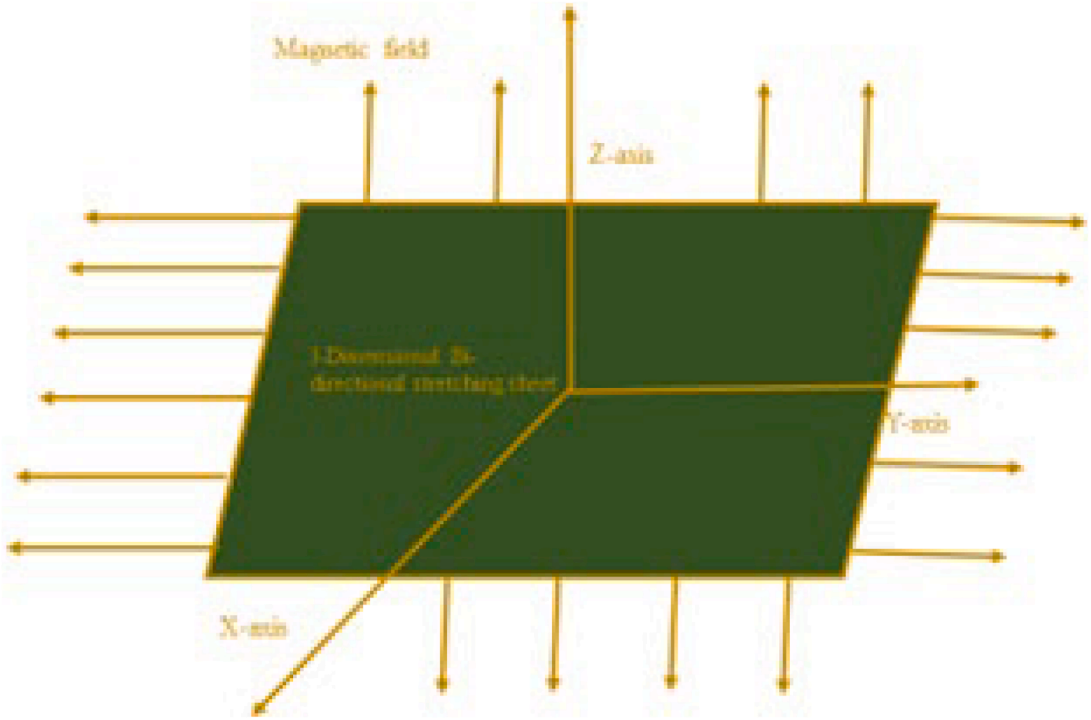

Fig. 1. Geometrical representation of flow model.

been presented on the impact of chemical reactions, demonstrating their usefulness in a variety of disciplines of science and industry [13]. Chemical process produces the combination between two or more substances, and can be occurs in the single phase (homogeneous) and different phase (heterogeneous). Other role in the chemical reaction are catalysts, and they have three types (positive, negative, or autocatalysis). The chemical process rate can be accelerated and slowed down by the positive catalyst and negative catalyst, respectively. Meanwhile, auto catalyst operates due to the condition that the mechanism aims to be achieved. The examples of catalysts are zeolites, aluminum chloride, hydrogen chloride, nickel, platinum, or palladium, etc. The numerical reports regarding autocatalysts and chemical processes have been published [14–17], where the fluid flow models described the effects of entropy generation [14,15], viscous dissipation [15], thermal relaxation and MHD flow [16,17], and cross flow [17].

The primary objective of this study is to formulate and solve a mathematical model describing the flow of a Carreau nanofluid influenced by a homogeneous–heterogeneous chemical reaction initiated through cubic autocatalysis. The model is considered within an inclined magnetized environment and incorporates velocity slip conditions along a bidirectionally stretching surface. Temperature variation within the fluid is governed by temperature-dependent thermal conductivity, while the thermal behavior is further modulated by internal heat generation effects.

2. The description of the problem formulation

The graphical representation of the model problem is illustrated in Fig. 1. There is considered an incompressible boundary layer and their dimensional Carreau nanofluid is flow with the effect of an magnetic field with 1st order rapidity slippage constraint over the bidirectional stretching sheet. Moreover, the isothermal cubic autocatalytic reaction is expressed by [18–21]

$$\left.\begin{array}{c}\overline{E}+2\overline{F}\rightarrow 3\overline{F}, \text{and its rate is given by}\\ \text{rate}=\overline{G}_a\overline{G}_b^{\,2}.\end{array}\right\} \tag{1}$$

While isothermal cubic autocatalytic reaction is presented as below:

$$\left.\begin{array}{c}\overline{E}\rightarrow\overline{F}, \text{and its rate is given by}\\ \text{rate}=\overline{k}_s\overline{G}_a.\end{array}\right\} \tag{2}$$

The flow range is between $z=0$ (minimum location) and $z>0$. To produce a constant temperature, the condition at the boundary must be convective. The fluid velocities in $x-$ axis and $y-$ axis are symbolized by $u_w(x)$ and $v_w(x)$, respectively. C_∞, C_w, T_∞, and T_f are ambient concentration, nanoparticles concentration, ambient temperatures, and temperatures, respectively.

$$\frac{\partial u}{\partial x}+\frac{\partial v}{\partial y}+\frac{\partial w}{\partial z}=0, \tag{3}$$

$$\frac{\partial u}{\partial t}+u\frac{\partial u}{\partial x}+v\frac{\partial u}{\partial y}+w\frac{\partial w}{\partial z}=-\frac{1}{\rho_f}\frac{\partial p}{\partial x}+\upsilon\frac{\partial}{\partial z}\left[\frac{\frac{\partial u}{\partial z}}{1+\left(\Gamma\frac{\partial u}{\partial z}\right)^n}\right]-\frac{\sigma_1 B_0^2\sin^2(\vartheta)}{\rho_f}u, \tag{4}$$

$$\frac{\partial v}{\partial t}+u\frac{\partial v}{\partial x}+v\frac{\partial v}{\partial y}+w\frac{\partial v}{\partial z}=-\frac{1}{\rho_f}\frac{\partial p}{\partial y}+\upsilon\frac{\partial}{\partial z}\left[\frac{\frac{\partial v}{\partial z}}{1+\left(\Gamma\frac{\partial v}{\partial z}\right)^n}\right]-\frac{\sigma_1 B_0^2\sin^2(\vartheta)}{\rho_f}v, \tag{5}$$

$$\frac{\partial T}{\partial t}+u\frac{\partial T}{\partial x}+v\frac{\partial T}{\partial y}+w\frac{\partial T}{\partial z}=\alpha_1\frac{\partial}{\partial z}\left\{K(T)\frac{\partial T}{\partial z}\right\}-\frac{k_1 G_a G_b^{\,2}}{(\rho c)_f}\left[-\frac{\Delta H_h}{\delta_A}\right]-\frac{1}{(\rho c)_f}\frac{\partial q_r}{\partial z}, \tag{6}$$

$$\frac{\partial G_a}{\partial t}+u\frac{\partial G_a}{\partial x}+v\frac{\partial G_a}{\partial y}+w\frac{\partial G_a}{\partial z}=D_A\frac{\partial^2 G_a}{\partial z^2}-k_1 G_a G_b^{\,2}, \tag{7}$$

$$\frac{\partial G_b}{\partial t}+u\frac{\partial G_b}{\partial x}+v\frac{\partial G_b}{\partial y}+w\frac{\partial G_b}{\partial z}=D_A\frac{\partial^2 G_b}{\partial z^2}-k_1 G_a G_b^{\,2}, \tag{8}$$

The boundary conditions are

$$\left.\begin{array}{c}u=u_w(x)+\gamma_0\frac{\partial u}{\partial z}, v=v_w(x)+\gamma_0\frac{\partial u}{\partial z}, w=0, C=C_w, -k_r\frac{\partial T}{\partial z}=k_s G_a\left[\frac{\Delta H_s}{\delta_A}\right]\\ D_A\frac{\partial G_a}{\partial z}+D_B\frac{\partial G_b}{\partial z}=k_s G_a \text{ at } z=0,\end{array}\right\} \tag{9}$$

here,

$$u_w(x,t)=\frac{ax}{1-\beta t},\ v_w(x,t)=\frac{ay}{1-\beta t}, \tag{10}$$

$$u\rightarrow 0, G_a\rightarrow G_\infty, C\rightarrow C_\infty, G_b\rightarrow 0, v\rightarrow 0, T\rightarrow T_\infty \text{ as } z\rightarrow\infty. \tag{11}$$

The appropriate conversions are introduces as below

$$\left.\begin{array}{c}\varphi(\eta)=\frac{G_b}{G_\infty}, \theta(\eta)=\frac{T-T_\infty}{\Delta T}, \phi(\eta)=\frac{G_a}{G_\infty}, w=\sqrt{\frac{va}{1-\beta t}}(f(\eta)+g(\eta))\\ u=\frac{ax}{1-\beta t}f'(\eta), v=-\frac{ay}{1-\beta t}g'(\eta), \eta=z\sqrt{\frac{a}{[1-\beta t]\nu}},\end{array}\right) \tag{12}$$

The subsequent set of ODEs are obtained, after implementing Eq. (12):

$$\left[1-\left(We_1 f''^2\right)\right]^{(n-3)/2}f'''+[(f+g)f'']\left(1+(We_1 f'')^n\right)^{(n-3)/2}-(1+(We_1 f'')^n)^2\left[S\left(f'+\frac{\eta}{2}f'\right)+f'^2+M^2\sin^2(\vartheta)f'\right]=0 \tag{13}$$

$$[1+(We_1 g'')]^{(n-3)/2}g'''+[(f+g)g'']\left(1+(We_1 g'')^n\right)^{(n-1)/2}-(1+(We_1 g'')^n)^2\left[S\left(g'+\frac{\eta}{2}g'\right)+g'^2+M^2\sin^2(\vartheta)g'\right]=0 \tag{14}$$

$$\frac{d}{d\eta}\left[\left(1+Rd\left(\theta_f-1\right)\theta\right)^3\theta'\right]+\Pr[\varepsilon\theta]\theta''+\Pr\varepsilon\theta'^2-\Pr\left[S\frac{\eta}{2}\theta'-R_H\varphi^2\phi-(f+g)\theta'\right]=0, \tag{15}$$

$$\phi''+S_c\left[(f+g)\phi'-K\varphi^2\phi-S\frac{\eta}{2}\phi'\right]=0, \tag{16}$$

$$\varphi''+S_c\left[(f+g)\varphi-K\varphi^2\phi-S\frac{\eta}{2}\varphi'\right]=0. \tag{17}$$

With the involvement of the below equations:

$$\phi+\varphi=1\Rightarrow\phi=1-\varphi \text{ or } \varphi=1-\phi \tag{18}$$

$$\phi''+S_c\left[(f+g)\phi'-K(1-\phi)^2\phi-S\frac{\eta}{2}\phi'\right]=0. \tag{19}$$

$$\varphi''+S_c\left[(f+g)\varphi-K(1-\phi)^2\phi-S\frac{\eta}{2}\varphi'\right]=0. \tag{20}$$

Then the final form of boundary constraints are

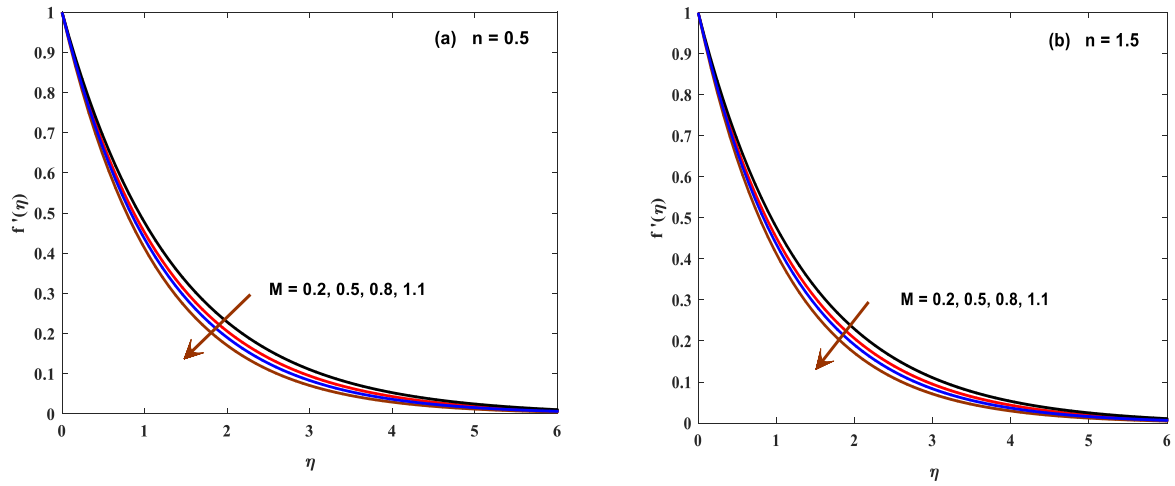

Fig. 2. (a and b). $f(\eta)$ against M.

$$\left.\begin{array}{c} f(0)=0, g(0)=0, \\ f'(0)=1+\gamma f''(0), g'(0)=\lambda+\gamma g''(0), \\ f(\infty)=0, f'(\infty)=0 \\ \theta'(0)=-K_r\phi(0), \phi'(0)+\varepsilon\varphi(0)=k_s\phi(0), \\ \theta(\infty)=0,\ \ \phi(\infty)=1 \end{array}\right\} \tag{21}$$

The parameters in the ODEs are:

$We_1 = \Gamma a x\left(\sqrt{\frac{a}{\nu(1-\beta t)}}\right)$, $We_2 = \Gamma a y\left(\sqrt{\frac{a}{\nu(1-\beta t)}}\right)$, $M = \frac{\sigma B_0^2}{\rho_f a}(1-\beta t)$, $R_d = \frac{16\sigma^* T_\infty^3}{3k^* k}$, $\Pr = \frac{\nu}{\alpha}$, $K = \frac{k_1 G_\infty{}^2}{a}(1-\beta t)$, $Sc = \frac{\nu}{D_A}$, $\gamma = \gamma_0\sqrt{\frac{a}{\nu}}$, $\lambda = \frac{b}{a}$, $\theta_f = \frac{T_w}{T_\infty}$, $S = \frac{\beta}{a}$, $\varepsilon = \frac{D_B}{D_A}$, $R_H = K_1\frac{\Delta H_h}{\delta_A}\frac{1}{(\rho c)_f}\frac{G_\infty{}^2}{a\Delta T}(1-\beta t)$, and $\phi+\varphi = 1$ is used.

The skin friction coefficient and Nusselt number are indicated as [22–24]

$$\left.\begin{array}{c} C_{fx}=\left(\frac{2\tau_{xz}}{\rho u^2}\right)\Rightarrow(Re_x)^{-0.5}C_{fx}=2f''(0)\left[1+(We_1 f''(0))^2\right]^{(n-1)/2}, \\ C_{fy}=\left(\frac{2\tau_{yz}}{\rho u^2}\right)\Rightarrow(Re_x)^{-0.5}C_{fy}=2g''(0)\left[1+(We_1 g''(0))^2\right]^{(n-1)/2}, \\ Nu_x=\left(\frac{xq_w}{k(T_f-T)}\right)\Rightarrow(Re_x)^{-0.5}Nu_x=-\theta'(0). \end{array}\right\} \tag{22}$$

The vectors form for related physical quantities is:

$$\begin{bmatrix} C_{fx}(\mathrm{Re}_x)^{-0.5} \\ C_{fy}(\mathrm{Re}_x)^{-0.5} \\ Nu_x(\mathrm{Re}_x)^{-0.5} \end{bmatrix} = \begin{bmatrix} 2f''(0)\left[1+\left(We_1 f''(0)^2\right)\right]^{(n-1)/2} \\ 2g''(0)\left[1+\left(We_1 g''(0)^2\right)\right]^{(n-1)/2}, \\ -\theta'(0) \end{bmatrix} \tag{23}$$

3. Results and discussion

The ODEs obtained are nonlinear, and will be solved through bvp4c coding in MATLAB software. This coding is developed by the concept of R-K numerical method. The current study implements the combination of artificial neural network and bvp4c method, to provide the numerical solutions on the Carreau nanofluid flow acted by the cubic autocatalysis, inclined magnetized environment, and bounded by the velocity slip. The temperature profile contain temperature-dependent thermal conductivity, whereas concentration profile has the component of homogeneous-heterogeneous chemical reactions. The outcomes are presented by the graphs and statistical tables, which governed by the related parameters. Thermal dispersion in the Carreau nanofluid are produced by heat generation. There are several parameters in the current study, namely as Weissenberg numbers, magnetic parameter, radiation parameter, Prandtl number, strength coefficient homogenous reaction, Schmidt number, velocity ratio, temperature ratio parameter, thermal conductivity, unsteadiness parameter, diffusion coefficient, homogenous reaction, and is Carreau fluid index. These are symbolized as following: We_1, We_2, M, R_d, Pr, K, Sc, λ, θ_f, K_r, S, ε, R_H, and n. Their impacts can be observed in the illustrations of temperature, velocity, and concentration. The velocity distributions depicted in Fig. 3(a and b) and S2 (a, b) illustrate the fundamental impact of non-Newtonian behavior and magnetic influence on fluid flow characteristics. In the shear-thinning (pseudoplastic) case, corresponding to $(0 < n < 1)$ the fluid

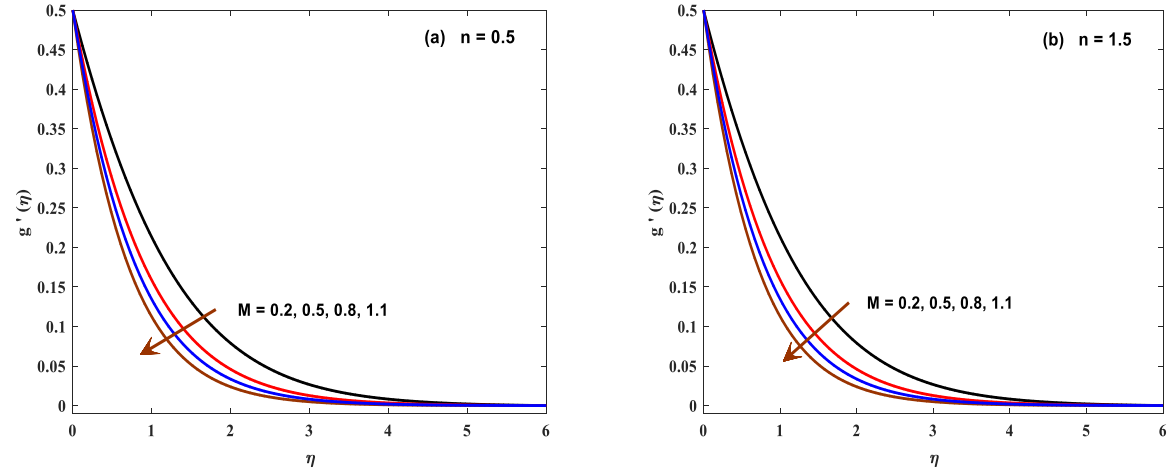

Fig. 3. (a and b). $g(\eta)$ against M.

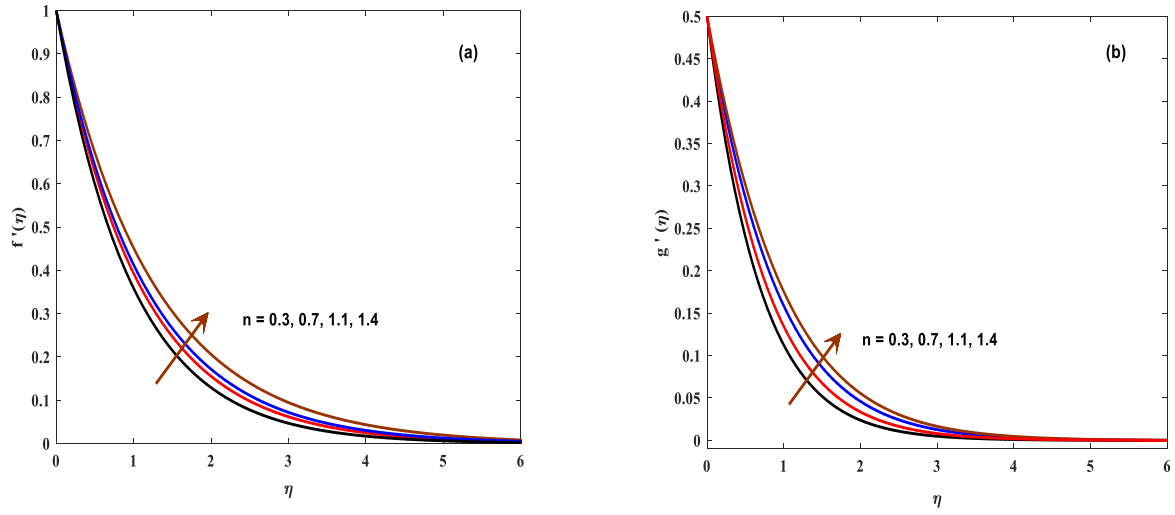

Fig. 4. (a and b). $f(\eta)$ and $g(\eta)$ against n.

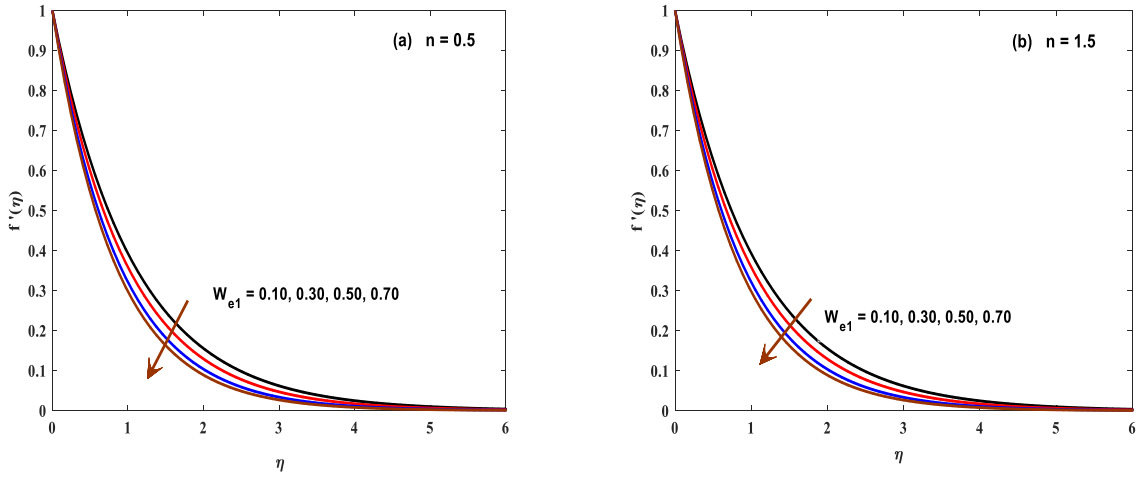

Fig. 5. (a and b). $f(\eta)$ against We_1.

exhibits reduced viscosity with increasing shear rate, allowing for enhanced velocity near the surface. Conversely, in the shear-thickening (dilatant) case with $(n > 1)$, the fluid becomes more resistant to flow under shear, resulting in a diminished velocity profile. The presence of a magnetic field introduces a Lorentz force that acts in the opposite direction to the flow, effectively damping the fluid motion. This magnetic resistance is more pronounced in the dilatant regime due to the inherently higher flow resistance, thereby significantly suppressing velocity. These findings are critical for optimizing flow control in magnetically influenced industrial and biomedical systems using non-Newtonian nanofluids. As a result, velocity is decreased due to magnetic field as shown in Fig. 2(a and b) and 3(a and b). The effect of the Carreau fluid index n on the velocity profile is illustrated in Fig. 4(a and b). Physically, the parameter n characterizes the shear-dependent viscosity behavior of the Carreau fluid. As the value of n increases, the fluid exhibits less shear-thinning behavior, resulting in a decrease in effective viscosity at moderate to high shear rates. This reduction in viscosity decreases the internal resistance to flow, thereby allowing the fluid to move more freely. Consequently, an increase in n leads to an enhancement in the velocity profile of the fluid. This behavior highlights the significant role of the fluid's rheological properties in controlling flow characteristics in non-Newtonian systems. Fig. 5(a and b) and S1(a, b) depict the behavior of the velocity profile with respect to the Weissenberg number We_1, We_2 for both pseudoplastic (shear-thinning) and dilatant (shear-thickening) cases. The Weissenberg number is a dimensionless parameter that represents the ratio of elastic (relaxation) forces to viscous forces in a viscoelastic fluid. Physically, a higher Weissenberg number indicates a greater influence of the fluid's memory effects or elasticity. As the values of We_1, We_2 increase, the relaxation time of the fluid becomes more dominant, meaning the fluid resists deformation more strongly due to its elastic nature. This resistance suppresses the fluid motion, thereby reducing the velocity distribution. Thus, in both pseudoplastic and dilatant regimes, an increase in the Weissenberg number leads to a noticeable decrease in velocity, emphasizing the retarding influence of fluid elasticity on the flow behavior. The temperature and concentration profiles depicted in Figures S2- S8 highlight the complex interplay between thermal diffusion, radiation, chemical reactions, and non-Newtonian behavior in Carreau nanofluids. Figure S2(a, b) illustrates the influence of the diffusion coefficient on the temperature distribution within the fluid. Physically, the diffusion coefficient quantifies the rate at which particles or molecules spread from one region to another. An increase in the diffusion coefficient enhances the rate of molecular transport, allowing species to move more rapidly from areas of lower concentration to higher concentration. This may seem counterintuitive, but in reactive or energy-coupled flows such as those involving nanofluids such movement can lead to intensified interactions between particles and the base fluid. These interactions generate additional thermal energy through mechanisms like Brownian motion and thermophoresis.

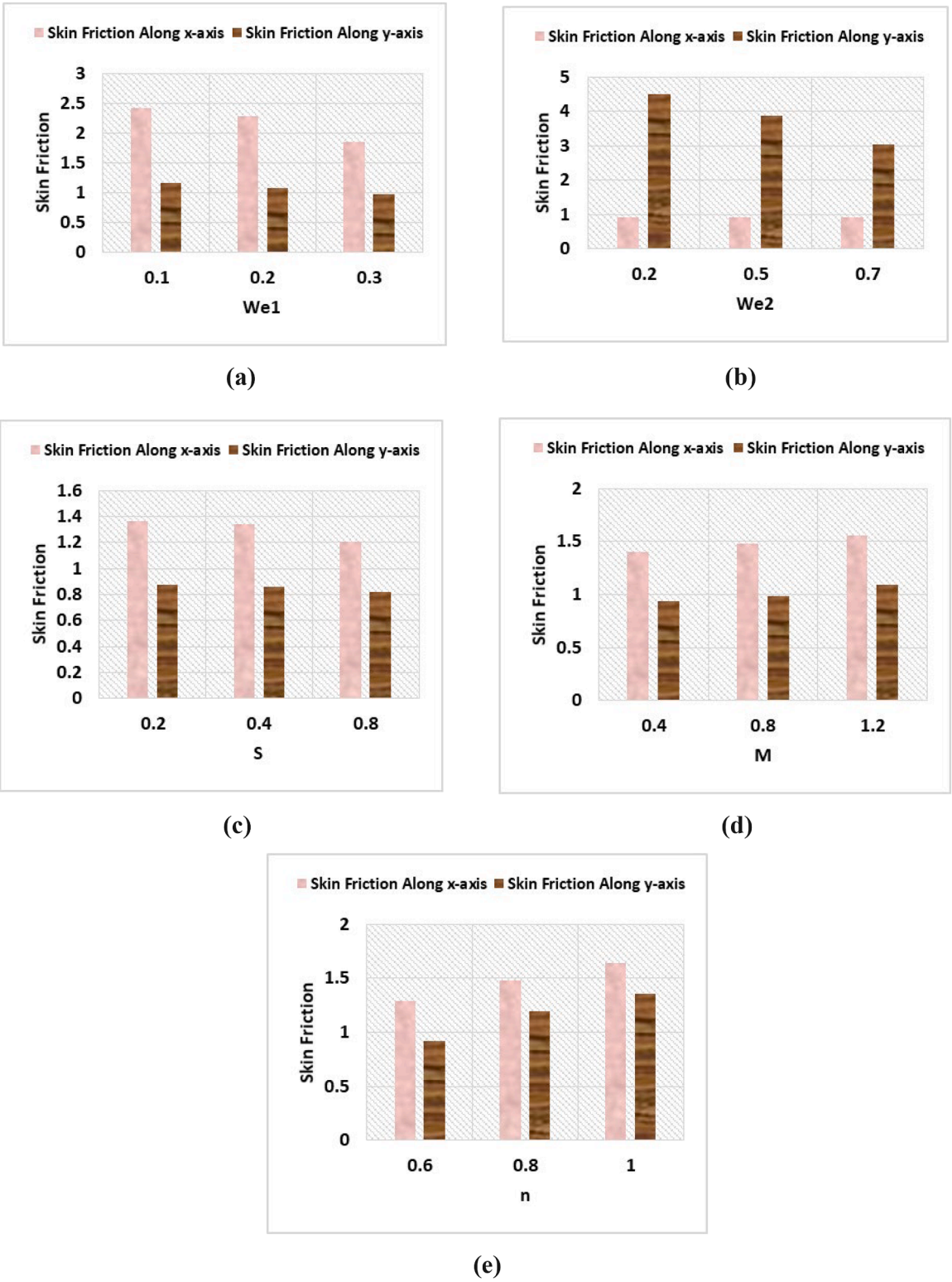

Fig. 6. (a–e). Bar graphs for local skin friction relates to We_1, We_2, M, n, and Sc.

Consequently, higher diffusion coefficients promote more efficient energy transfer within the fluid, leading to an overall rise in temperature, especially when strong concentration gradients are present. This coupling between mass and heat transfer emphasizes the role of molecular diffusion in enhancing thermal performance in such fluid systems. As shown in Figure S3(a, b), an increase in the Prandtl number Pr leads to a noticeable reduction in the temperature distribution within the fluid. Physically, the Prandtl number is defined as the ratio of momentum diffusivity (kinematic viscosity) to thermal diffusivity. It characterizes the relative thickness of the velocity boundary layer compared to the thermal boundary layer. A higher Pr indicates that momentum diffuses much faster than heat, meaning the fluid has a lower capacity to conduct thermal energy. As a result, thermal diffusion becomes weaker, and heat remains confined near the surface or source,

Table 1
The numerical values of skin friction for the 2D axes $x-$ and $y\ -$.

We_1	We_2	S	M	n	Frictional force along $x-$ axis	Frictional force along $y-$ axis
0.10					2.4234169	1.1700415
0.20					2.2824937	1.0703786
0.30					1.8463254	0.9817985
0.50	0.20				0.9144275	4.4910224
	0.50				0.9135998	3.8765338
	0.70				0.9130784	3.0329594
		0.20			1.3601325	0.8749739
		0.40			1.3426635	0.8572848
		0.80			1.2022842	0.8178665
			0.40		1.3964775	0.9344596
			0.80		1.4810632	0.9847028
			1.20		1.5573543	1.0945558
				0.60	1.2853425	0.9205395
				0.80	1.473908	1.197946
				1.00	2.639188	1.354682

Table 2
Pr, We_1, Sc, We_2, S and n implication on Nusselt number.

Pr	Sc	We_1	We_2	S	n	Nusselt Number
0.10						0.002131929
0.20						0.002131254
0.30						0.002130059
0.50	0.30					0.004388564
	0.60					0.006516988
	0.90					0.007383849
		0.70				0.003093628
		0.90				0.003084859
		1.10				0.003076849
			0.70			0.003125289
			0.90			0.003121295
			1.10			0.003117249
				0.70		0.003081969
				0.90		0.003055814
				1.20		0.003028675
					0.40	0.003177036
					0.70	0.003229315
					1.10	0.003226135

causing a thinner thermal boundary layer. This restriction in thermal transport leads to a decrease in the overall temperature within the fluid domain. Therefore, fluids with higher Prandtl numbers such as oils exhibit lower thermal conductivity and thus lower temperature profiles compared to fluids with lower Pr values, such as gases or water. Figure S4(a, b) reveals that stronger thermal radiation significantly raises the fluid temperature due to increased radiative heat energy absorption. Furthermore, Figure S5(a, b) indicates that the homogeneous chemical reaction promotes temperature enhancement, as it involves interaction between nanoparticles and the base fluid, intensifying internal heat generation.

Figures S6–S8 demonstrate that the diffusion parameter has a significant positive effect on nanoparticle concentration within the boundary layer in both pseudoplastic (shear-thinning) and dilatant (shear-thickening) flow regimes. Physically, the diffusion parameter characterizes the rate at which nanoparticles spread due to concentration gradients. An increase in this parameter enhances molecular and particle mobility, allowing nanoparticles to diffuse more effectively from high-concentration regions toward areas of lower concentration. In both types of non-Newtonian fluids, this intensified diffusive transport leads to an accumulation of nanoparticles within the boundary layer. This behavior plays a critical role in systems where precise control over particle distribution is essential. For instance, in drug delivery applications, efficient diffusion ensures targeted delivery and sustained release; in thermal energy storage, higher nanoparticle concentration enhances thermal conductivity; and in chemical reactors, improved mass transport supports faster reaction rates. Thus, understanding the influence of the diffusion parameter is vital for optimizing performance in these advanced engineering and biomedical systems.

The strength coefficient homogenous reaction parameter is responsible for decreasing the concentration distribution, as presented in Figure S7 (a, b). Besides, the concentration distribution is enhanced due to the numerical values of Schmidt quantity Sc, as shown in Figure S8 (a, b). The figure (a) displays the shear thinning case, whereas (b) illustrates the shear thickening case.

(Figs 6- S9), each of them have their figures as in (a-e) show the effect of the related physical parameters on the local skin friction and Nusselt number, respectively. The numerical outcomes for local skin friction is tabulated in Table 1, whereas the tabulation of Nusselt number is shown in Table 2.

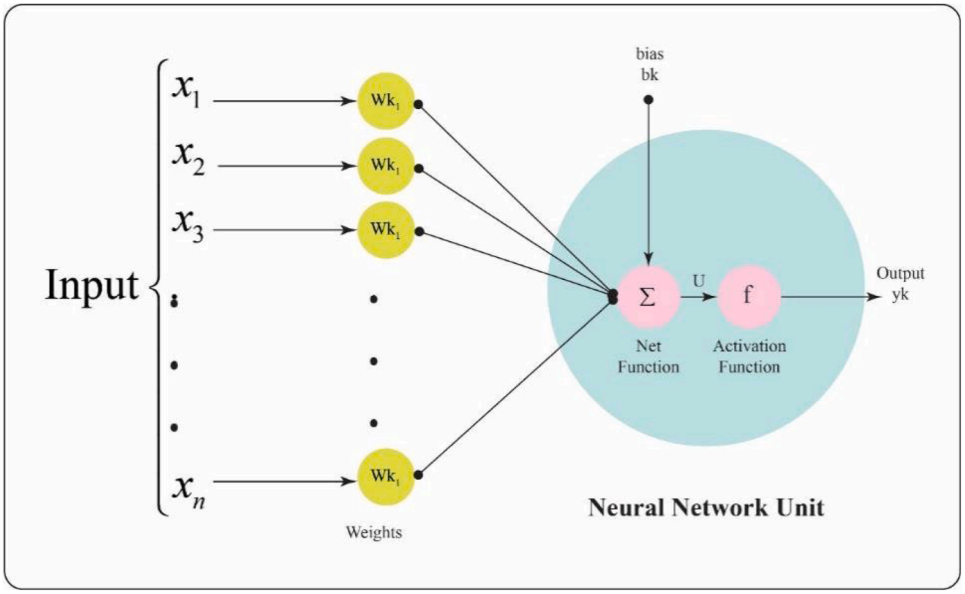

Fig. 7. An illustration of a single neural model.

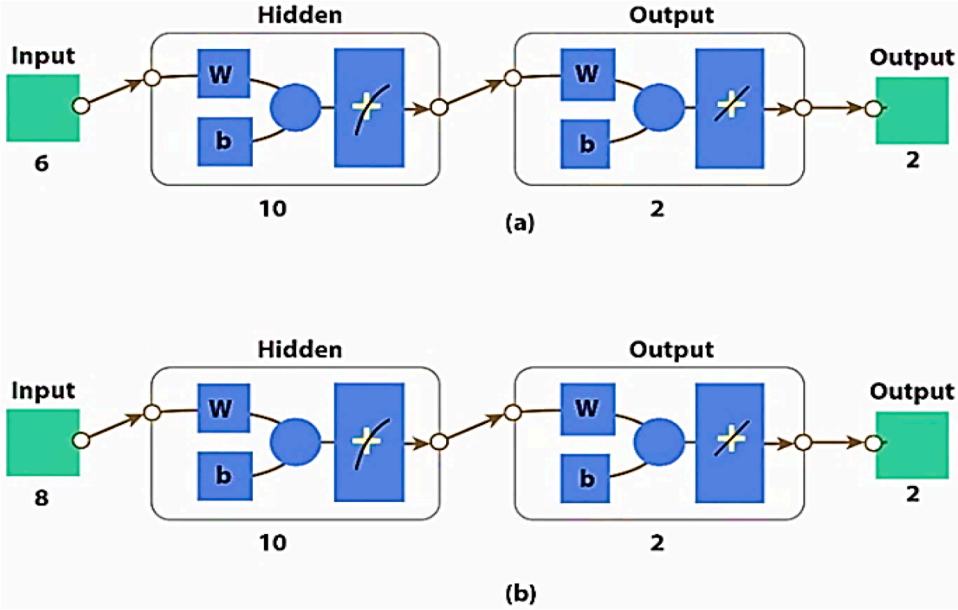

Fig. 8. (a and b). ANNs configuration.

Table 3
Achievement for Scenario 1: Carreau nanofluidic model.

State of problem	Obtained Mean square error for different cases			Production	Gradientnumerical	Mu	Epoch	Time taken
	Numerical values of Training	Validation process	Numerical Testation					
1.0	3.098×10^{-10}	5.41×10^{-10}	3.54×10^{-8}	3.10×10^{-10}	9.80×10^{-8}	1.0×10^{-8}	255	2.0
2.0	1.75×10^{-9}	3.31×10^{-9}	2.89×10^{-9}	1.73×10^{-9}	9.94×10^{-8}	1.0×10^{-8}	217	1.0
3.0	1.16×10^{-9}	1.85×10^{-9}	2.25×10^{-7}	1.14×10^{-9}	9.92×10^{-8}	1.0×10^{-8}	269	1.0

Table 4
Outcomes of NN-BLMS for Scenario 2: Carreau magneto-nanofluidic model.

State of problem	Obtained Mean square error for different cases			Presentation	Gradient	Mu	Epoch	Time
	Numerical values of Training	Validation	Testation occurrence					
1.0	1.040×10^{-10}	6.490×10^{-9}	9.850×10^{-8}	1.040×10^{-10}	9.990×10^{-8}	1.001×10^{-9}	412	2
2.0	3.690×10^{-9}	1.240×10^{-8}	1.320×10^{-8}	3.680×10^{-9}	9.950×10^{-8}	1.001×10^{-9}	150	1
3.0	2.770×10^{-9}	9.640×10^{-8}	7.710×10^{-9}	2.770×10^{-9}	9.960×10^{-8}	1.001×10^{-8}	188	0

4. Artificial neural network

This section deals with the discussion regarding ANN scheme. Fig. 7 interprets intelligent computation of neuron prototypical incorporated to improve the suggested network. Fig. 8(a–F) also probed its mechanism. Figures S10–9 are established for γ with attached temperature. The numerical values of the implementation of NN-BLMS for all the scenarios are tabulated in Tables S1- S4, respectively. The specific cases for all the tables are listed as below: a) types of scenarios (1–6) for the Carreau nanofluid model (Table S1), b) Scenario 1: Carreau nanofluidic model (Table 3), c) Scenario 2: Carreau magneto-nanofluidic model (Table 4), d) Scenario 3: cross magneto-nanofluidic model (Table S2), e) Scenario 4: cross nanofluidic model (Table S3), f) Scenario 5: cross magneto-nanofluidic model (Table S4).

A single structured neural model for the proposed NN-BLMS scheme is presented in Fig. 7. NN-BLMS is being utilized by a neural network fitting tool ('nftool'). The development of neural networks is regarding the backpropagation of Levenberg-Marquardt. Implementation of NN-BLMS contains six scenarios, which are varied by parameters *Rd*, *Pr*, λ, *Nt*, *Nb*, γ . In addition, the group of the three cases in EPNFM have constant values.

Formulated Table 3 corresponds to all six Cases. Reference data and its step size for NN-BLMS scheme are 0 until 4 and 0.04, respectively. The solution is obtained by the built-in command 'NDSolve'. For 101 input points, the dataset values for, f', g, θ, and ϕ are trained with 70 %, validated with 15 %, and tested with 15 %. The scheme NN-BLMS is basically dependent upon the computing paradigm as shown in Fig. 8(a and b). All Fig. 9(a–F) are established for showing the convergence of MSE for train, validation, and test procedures. The assumed network achieved performance at 254, 167, 161, 113, 222, and 390 epochs. Fig. 10(a-F) is described to show the state transition dynamics of the Carreau fluidic model. Accuracy of results is hereby achieved for each Case. Fig. 11-S14 are presented for Case 2 of all six Scenarios. For error dynamic input between 0 and 4 is taken and 0.04 is the step size. Evaluation of error analysis is presented by histograms and related figures are plotted and tabulated for the second case, and subjected to all scenarios (Fig. 12(a-F) and Tables S1-S4).

5. Final remarks

The study analyzes the inclined magnetohydrodynamic flow of Carreau nanofluids, incorporating cubic autocatalysis and chemical reactions. It uses artificial neural networks to capture nonlinear behavior and validates predictions, providing insight into transport phenomena in

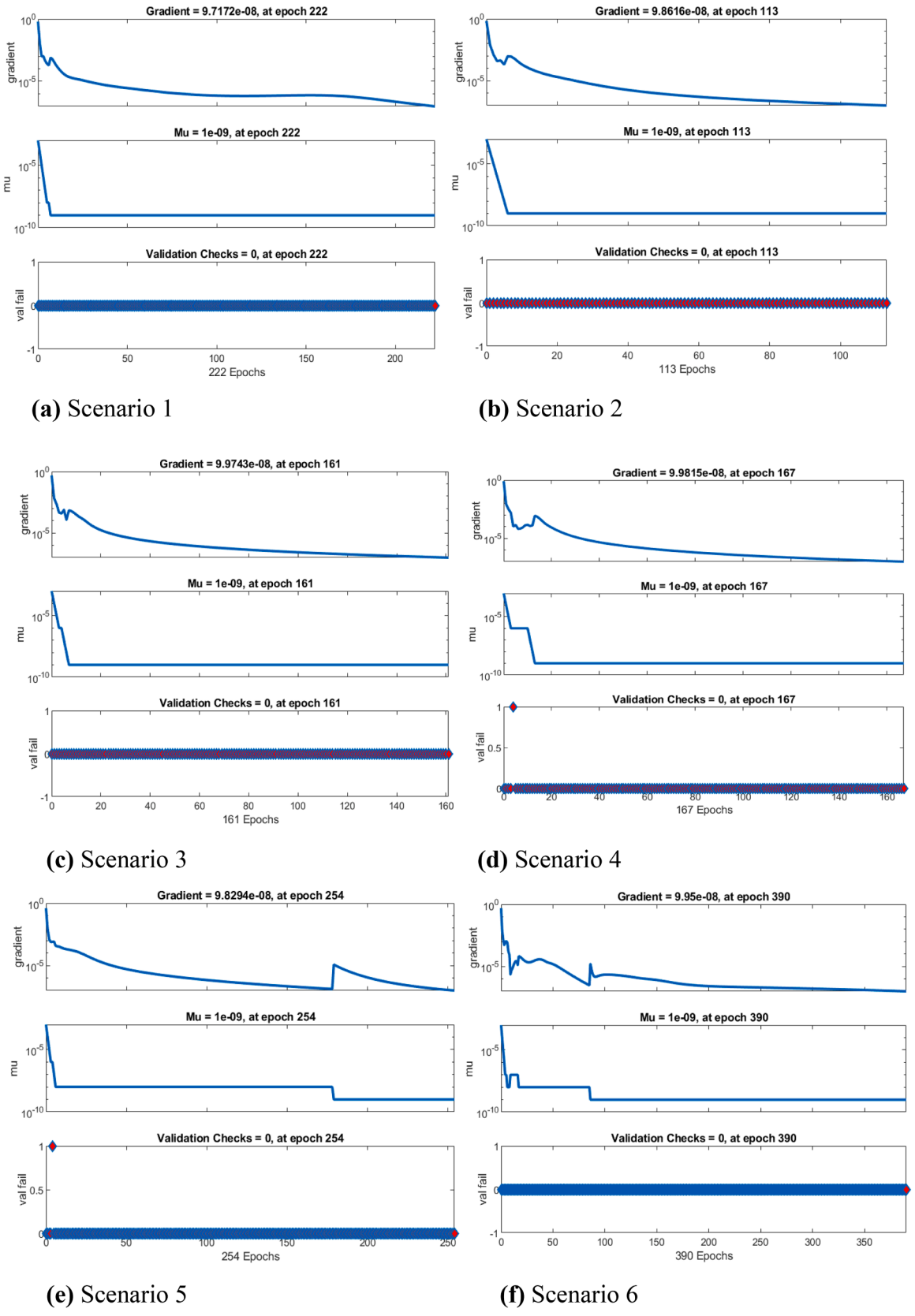

Fig. 9. (a–f). State transition Case 2: dynamics of Carreau fluidic model.

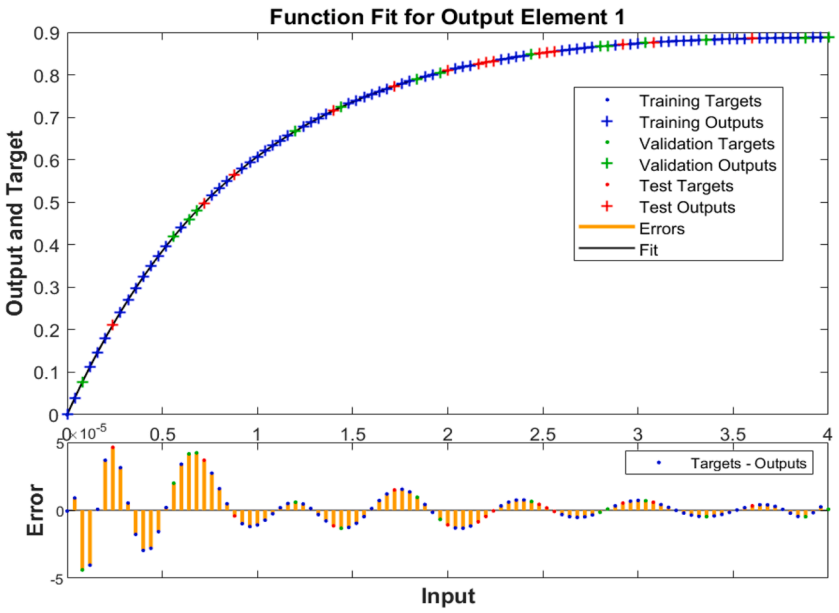

Fig. 10. The NN-BLMS result is compared with the attachment of Case 2, Scenario 1: CFMNM.

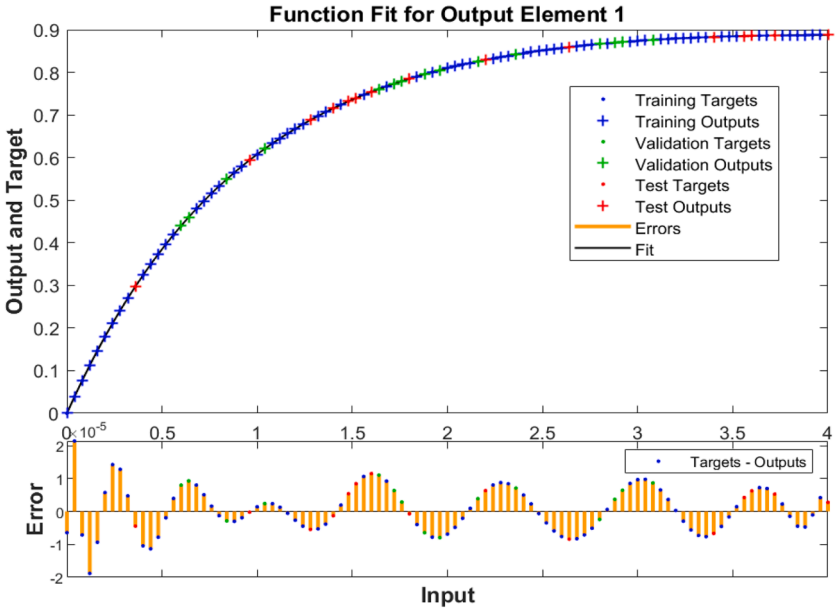

Fig. 11. The NN-BLMS result is compared with the attachment of Case 2, Scenario 2: CFMNM.

non-Newtonian fluids.

The outcomes of this research study can be concluded as follows:

i. For the cases of pseudoplasticity and dilatant, the diffusion of nanoparticles cause the nanofluid temperature to be increased. The movement of these nanoparticles can be described from the process of homogenous reaction, where this reaction is involved in the heat transfer process of the Carreau nanofluid.
ii. However, the process of homogenous reaction parameter is responsible to decrease the concentration distribution.
iii. The slower rate of velocity is due to the intensified magnetic field, since this field generates the Lorentz force and this force opposes the flow.
iv. When *n* increases, then velocity distribution is increasing.
v. The temperature gradient causes the diffusion of the molecules from the lower concentration region, to high concentration region.
vi. For the cases of pseudoplasticity and dilatant in the Carreau nanofluid, temperature is decreased when *Pr* is rising.
vii. Temperature is enhanced as thermal radiation is increased.
viii. The enhancement concentration distribution of Carreau fluid for pseudoplasticity and dilatant models is caused by the diffusion parameter.

CRediT authorship contribution statement

Nek Muhammad Katbar: Investigation. **Hina Zahir:** Methodology. **Kamel Guedri:** Writing – original draft, Project administration. **Basim M. Makhdoum:** Validation, Funding acquisition. **Siti Suzilliana Putri Mohamed Isa:** Visualization. **Syed M. Hussain:** Resources, Data

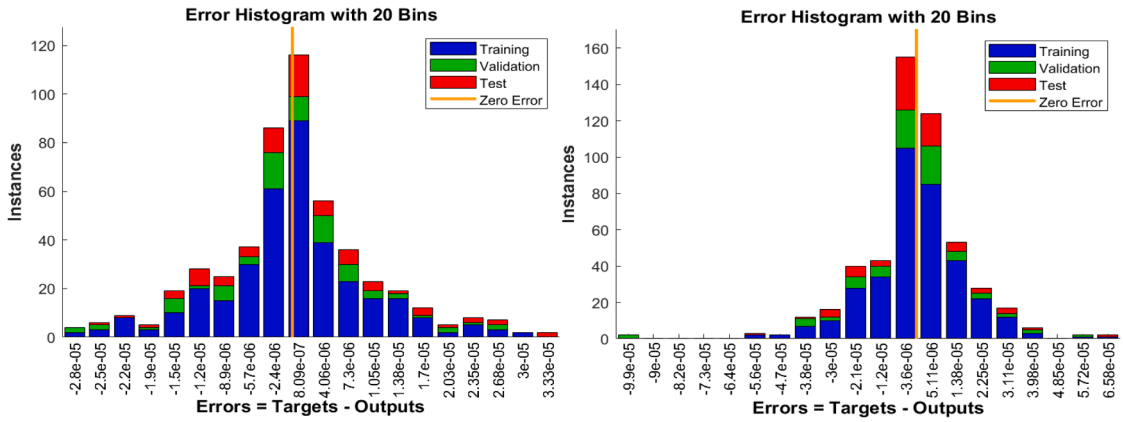

(a) Case 2 and Scenario 1. **(b)** Case 2 and Scenario 2.

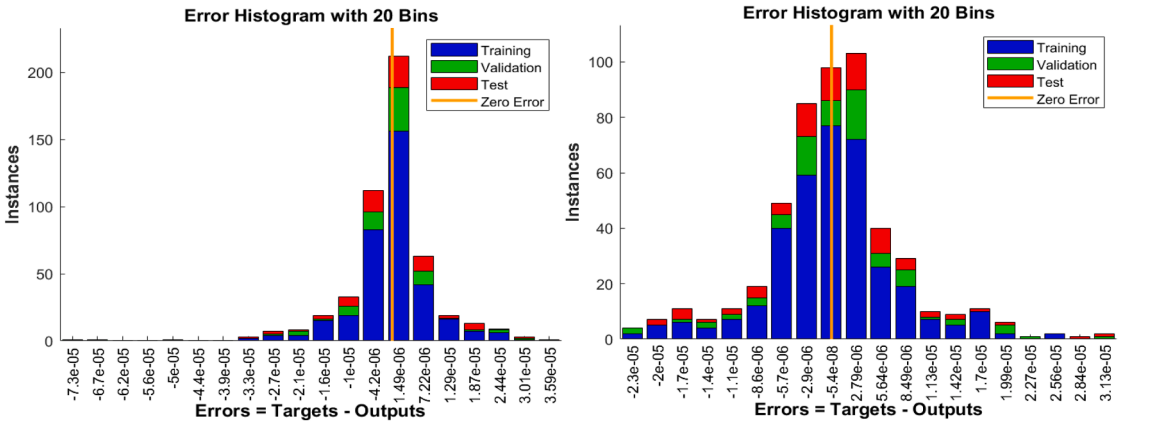

(c) Case 2 and Scenario 3. **(d)** Case 2 and Scenario 4.

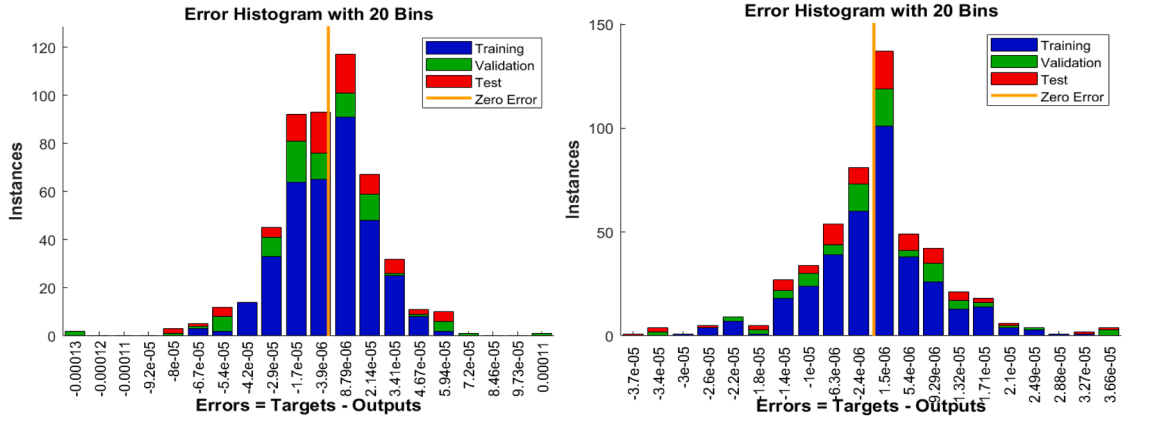

(e) Case 2 and Scenario 5. **(f)** Case 2 and Scenario 6.

Fig. 12. (a–f). Error analysis with help of a histogram considering Case 2 and Scenario 6.

curation, Conceptualization. **Abbas Khan:** Visualization, Methodology, Funding acquisition.

Declaration of competing interest

The authors declare that they have no known competing financial interests or personal relationships that could have appeared to influence the work reported in this paper.

Availability of data and material

All data generated or analyzed during this study are included in this published article.

Supplementary materials

Supplementary material associated with this article can be found, in the online version, at doi:10.1016/j.rineng.2025.106598.

Data availability

Data will be made available on request.

References

[1] W. Jamshed, et al., Partial velocity slip effect on working magneto non-newtonian nanofluids flow in solar collectors subject to change viscosity and thermal conductivity with temperature, PLoS One 16 (2021) e0259881, https://doi.org/10.1371/journal.pone.0259881.

[2] M.R. Eid, F. Mabood, Two-phase permeable non-Newtonian cross-nanomaterial flow with Arrhenius energy and entropy generation: darcy-Forchheimer model, Phys. Scr 95 (2020) 105209, https://doi.org/10.1088/1402-4896/abb5c7.

[3] P.J. Carreau, Rheological equations from molecular network theories, Trans. Soc. Rheol. 16 (1) (1972) 99–127, https://doi.org/10.1122/1.549276.

[4] H.A. Nabwey, S.I. Alshber, A.M. Rashad, A.E.N. Mahdy, Influence of bioconvection and chemical reaction on magneto—Carreau nanofluid flow through an inclined cylinder, Mathematics 10 (3) (2022) 504, https://doi.org/10.3390/math10030504.

[5] M. Ramzan, et al., Computational assessment of microrotation and buoyancy effects on the stagnation point flow of Carreau–Yasuda hybrid nanofluid with chemical reaction past a convectively heated Riga plate, ACS. Omega 7 (34) (2022) 30297–30312, https://doi.org/10.1021/acsomega.2c03570.

[6] K.U. Rehman, W. Shatanawi, K. Abodayeh, A group theoretic analysis on heat transfer in MHD thermally slip Carreau fluid subject to multiple flow regimes (MFRs), Case Stud. Therm. Eng. 30 (2022) 101787, https://doi.org/10.1016/j.csite.2022.101787.

[7] K. Hosseinzadeh, et al., Investigation of cross-fluid flow containing motile gyrotactic microorganisms and nanoparticles over a three-dimensional cylinder, Alex. Eng. J. 59 (5) (2020) 3297–3307, https://doi.org/10.1016/j.aej.2020.04.037.

[8] T. Hayat, M.I. Khan, M. Tamoor, M. Waqas, A. Alsaedi, Numerical simulation of heat transfer in MHD stagnation point flow of Cross fluid model towards a stretched surface, Results. Phys. 7 (2017) 1824–1827, https://doi.org/10.1016/j.rinp.2017.05.022.

[9] M. Waqas, Simulation of revised nanofluid model in the stagnation region of cross fluid by expanding-contracting cylinder, Int. J. Numer. Meth. Heat Fluid Flow 30 (2020) 2193–2205, https://doi.org/10.1108/HFF-12-2018-0797.

[10] F. Sultan, W.A. Khan, M. Ali, M. Shahzad, M. Irfan, M. Khan, Theoretical aspects of thermophoresis and brownian motion for three-dimensional flow of the cross fluid with activation energy, Pramana 92 (2) (2019) 1–10, https://doi.org/10.1007/s12043-018-1676-0.

[11] S. Shaw, S. Samantaray, A. Misra, M.K. Nayak, O.D. Makinde, Hydromagnetic flow and thermal interpretations of Cross hybrid nanofluid influenced by linear, nonlinear and quadratic thermal radiations for any Prandtl number, Int. Commun. Heat Mass Transf. 130 (2022) 105816, https://doi.org/10.1016/j.icheatmasstransfer.2021.105816.

[12] M.R. Eid, K.L. Mahny, A.F. Al-Hossainy, Homogeneous-heterogeneous catalysis on electromagnetic radiative Prandtl fluid flow: darcy-Forchheimer substance scheme, Surf. Interf. 24 (2021) 101119, https://doi.org/10.1016/j.surfin.2021.101119.

[13] T.H. Alarabi, A.M. Rashad, M. Mahdy, Homogeneous–heterogeneous chemical reactions of radiation hybrid nanofluid flow on a cylinder with joule heating: nanoparticles shape impact, Coatings 11 (2021) 1490, https://doi.org/10.3390/coatings11121490.

[14] M.I. Khan, S.A. Khan, T. Hayat, S. Qayyum, A. Alsaedi, Entropy generation analysis in MHD flow of viscous fluid by a curved stretching surface with cubic autocatalysis chemical reaction, Eur. Phys. J. Plus 135 (2) (2020) 1–17, https://doi.org/10.1140/epjp/s13360-019-00030-1.

[15] M. Waqas, A mathematical and computational framework for heat transfer analysis of ferromagnetic non-Newtonian liquid subjected to heterogeneous and homogeneous reactions, J. Magn. Magn. Mater. 493 (2020) 165646, https://doi.org/10.1016/j.jmmm.2019.165646.

[16] U. Ali, M.Y. Malik, K.U. Rehman, M.S. Alqarni, Exploration of cubic autocatalysis and thermal relaxation in a non-Newtonian flow field with MHD effects, Phys. A 549 (2020) 124349, https://doi.org/10.1016/j.physa.2020.124349.

[17] Y.M. Chu, M.I. Khan, M.I. Ur Rehman, S. Kadry, M.K. Nayak, Flow and thermal management of MHD Cross nanofluids over a thin needle with auto catalysis chemical reactions, Int. J. Mod. Phys. B 34 (30) (2020) 2050287, https://doi.org/10.1142/S0217979220502872.

[18] K. Ramesh, F. Mebarek-Oudina, B. Souayeh, Mathematical Modelling of Fluid Dynamics and Nanofluids, CRC Press, Taylor & Francis Group, 2024.

[19] J. Raza, F. Mebarek-Oudina, H. Ali, I.E. Sarris, I. E, Slip effects on casson nanofluid over a stretching sheet with activation energy: RSM analysis, Front. Heat Mass Transf. 22 (4) (2024) 1017–1041.

[20] M.A. Kumar, F. Mebarek-Oudina, P. Mangathai, N.A. Shah, C. Vijayabhaskar, N. Venkatesh, Y. Fouad, The impact of Soret Dufour and radiation on the laminar flow of a rotating liquid past a porous plate via chemical reaction, Mod. Phys. Lett. B 39 (10) (2025) 2450458.

[21] J. Raza, F. Mebarek-Oudina, L.Ali Lund, The flow of magnetised convective Casson liquid via a porous channel with shrinking and stationary walls, Pramana 96 (4) (2022) 229.

[22] S. Ahmad, S. Mehfuz, F. Mebarek-Oudina, J. Beg, RSM analysis based cloud access security broker: a systematic literature review, Clust. Comput. 25 (5) (2022) 3733–3763.

[23] A. Shafiq, F. Mebarek-Oudina, T.N. Sindhu, G. Rasool, Sensitivity analysis for Walters-B nanoliquid flow over a radiative Riga surface by RSM, Sci. Iran. 29 (3) (2022) 1236–1249.

[24] C. Berkenkotter, T.N. Huckin, T. N, You are what you cite: novelty and intertextuality in a biologist's experimental article. Genre Knowledge in Disciplinary Communication, Routledge, 2016, pp. 45–60.